Theoretical and Applied Climatology (2019) 138:1795–1808
https://doi.org/10.1007/s00704-019-02937-2

ORIGINAL PAPER

# Intensity and spatial heterogeneity of design rainstorm under nonstationarity and stationarity hypothesis across mainland China

Zhaoyang Zeng[1] · Chengguang Lai[1,2] · Zhaoli Wang[1,2] · Xiaohong Chen[3] · Zhenxing Zhang[4] · Xiangju Cheng[1,2]

Received: 11 January 2019 / Accepted: 28 June 2019 / Published online: 9 July 2019


## Abstract

Understanding the trend characteristics of design rainstorm and spatial heterogeneity of extreme precipitation is of great importance to reduce disasters induced by rare extreme precipitation. Using a high-resolution (0.5° × 0.5°) daily gridded data set of precipitation across mainland China from 1961 to 2013, this study investigated the historical changing trend and spatial heterogeneity of design rainstorm using the 30-year moving window method (30YM). Differences in the quantification of the design rainstorm were compared for the use of the 30YM and the 30-year-based increasing window method (30YBI). The results show that a significant increasing intensity but no spatially uniform trend of design rainstorm can be observed across mainland China based on the 30YM analysis. The south, east, and northeast China mainly showed an increasing trend, but the southwest and north China presented a decreasing trend. The spatial heterogeneity of the design rainstorm was greatly enhanced if the nonstationarity assumption was adopted on the national scale. The heterogeneity showed an increasing trend mainly in southeast, north, northeast, and northwest China, and a decreasing trend in southwest and west China, indicating significant regional variation in spatial heterogeneity. For most areas of mainland China, especially for southeastern, northeastern, and western China, use of the most recent precipitation sub-series to quantify the design rainstorm may weaken the potential nonstationarity and guarantee the safety of infrastructure in these areas where design rainfall increases.

**Highlight**

1. Obtain a design rainstorm value using a 30-year moving window
2. Investigate the changing trend of design rainstorm across mainland China
3. Explore the spatial heterogeneity trend of design rainstorm across mainland China
4. Discuss the difference of design rainstorm from different amounts of rainfall data.

**Electronic supplementary material** The online version of this article (https://doi.org/10.1007/s00704-019-02937-2) contains supplementary material, which is available to authorized users.

✉ Zhaoli Wang
wangzhl@scut.edu.cn

[1] School of Civil Engineering and Transportation, South China University of Technology, Guangzhou 510641, China

[2] State Key Lab of Subtropical Building Science, South China University of Technology, Guangzhou 510641, China

[3] Center of Water Resources and Environment, Sun Yat-Sen University, Guangzhou 510275, China

[4] The Prairie Research Institute, University of Illinois at Urbana-Champaign, 2204 Griffith Drive, Champaign, IL 61820, USA

## 1 Introduction

Extreme weather and climate events have happened frequently in recent decades due to the changes of global warming, which is now one of the greatest threats to humans (Meehl et al. 2000; IPCC 2007, 2012; Stocker et al. 2013; Wang et al. 2017b; 2018a, b). Among these extreme weather and climate events, extreme precipitation is a common meteorological disaster with great potential harm that can also serve as a major trigger of many natural disasters, such as flash floods, urban waterlogging, landslides, and debris flow (Goswami et al. 2006; Parmesan 2006; Kendon et al. 2014; Wang et al. 2015; Yin et al. 2015; Fischer and Knutti 2016; Lai et al. 2016; Bao et al. 2017; Stennett-Brown et al. 2017). Many studies have indicated that both the frequency and intensity of extreme precipitation events in recent decades are exhibiting an increasing trend in most regions, including two-thirds of data-covered parts of Northern Hemisphere land areas (Min et al. 2011), southern Africa (Pinto et al. 2016), south-east Australia (Evans et al. 2017), and even areas where the mean (or total) precipitation showed a decreasing trend (Sillmann et al. 2017; Donat et al. 2017). The annual maximum daily precipitation in most of the above regions is expected to increase in the future (Rashid et al. 2016; Pinto et al. 2016; Evans et al. 2017), potentially due to human-induced climate change (Zhang et al. 2007; Westra et al. 2013; Ummenhofer and Meehl 2017). Thus, the variation characteristic of this meteorological disaster requires further attention.

The study of nonstationarity and spatial heterogeneity is a research priority in current efforts to understand extreme precipitation (Milly et al. 2008; Knutson et al. 2010; Ghosh et al. 2012; Burt et al. 2016; Son et al. 2017; Um et al. 2017). For the nonstationarity problem, it is generally thought that climate change and human activities disturbed the precipitation series (Du et al. 2015; Gu et al. 2016; Sraj et al. 2016; Cancelliere 2017; Gu et al. 2017a, b; Sun et al. 2017a). In this model, climate change and human activities have changed the atmospheric circulation and then altered the spatial-temporal characteristics of rainfall. The design rainstorm value may be underestimated if we adopt the stationarity assumption for a series (i.e., directly using the complete time series), especially for regions exhibiting increasing frequency and intensity of extreme precipitation (Lima et al. 2016; Singh et al. 2016; Zhang et al. 2017; So et al. 2017). There may be significant problems if the design rainstorm value fails to satisfy the expected standard, potentially resulting in disaster in new hydraulic engineering projects (e.g., dam break and levee failure). The safety of old hydraulic engineering structures may also decrease with time due to two reasons: (1) the so-called design standard based on a relatively short time series would decrease as the series length increases with more extreme values added to the series, and (2) with time, the stationarity of the series may be disturbed, mainly indicated by differences in the new series that the old series used to calculate the initial design standard for the hydraulic engineering project; these differences may be due to climate change and human activities. As an example, a dam may be constructed based on the flood control standard of a 100-year return period. However, after many years, the standard may become only an 80-year return period or an even shorter length of time to consider the above factors, and in this new analysis, the dam safety may greatly decrease. Accordingly, understanding the difference between the calculations of design rainstorm under nonstationarity and stationarity hypothesis is of great importance.

The spatial characteristics of extreme precipitation are usually different due to various geographical and climatic factors, especially for large regions or countries (e.g., USA, China, and India) featuring obviously different geographic and climate characteristics, presenting an obvious spatial heterogeneity problem (Ghosh et al. 2012; Choi et al. 2014; Liu et al. 2015; Singh and Goyal 2016; Sun et al. 2017b). To facilitate calculation under these conditions, the design rainstorm typically applies the same method throughout a region considered a homogeneous region (e.g., an administrative region, such as a city or even a country), ignoring any spatial heterogeneity of the design rainstorm. Hence, even if we have considered the influence of nonstationarity and series length, the actual standard may also be lower than the expected design standard in some local regions because the uniform design standard may not be completely appropriate to regions with spatially different precipitation characteristics. Therefore, spatial heterogeneity is another significant factor which can be used to calculate the appropriate design standard value, and understanding the trend of spatial heterogeneity can help to adjust measures in determining design rainstorm value, formulating water resource management, and preventing and mitigating disaster (Liu et al. 2014).

In mainland China, many cities have suffered disasters induced by extreme precipitation, causing huge economic losses, and casualties (Hu et al. 1998; Zong and Chen 2000; Wong and Zhao 2001; Cong et al. 2009; Zhang et al. 2013; Liu et al. 2015). For example, in 2012, Beijing city suffered the heaviest rainstorm (local areas reached the 500-year return period) and floods in the previous 61 years, causing submersion of 16,000 $km^2$ and more than 11.6 billion Yuan (equal to 1.8 billion dollars) in losses, and affecting 1.9 million people, with 79 deaths. In 2016, the rainfall depth in Wuhan city reached 315.8 mm from June 30 to July 2, one-third of the total annual rainfall, causing more than 30 deaths (Dai et al. 2017). Considering the seriousness of the disasters (e.g., floods, waterlogging, and landslides) that are related to rare extreme precipitation, there has been increased attention focused on the recent extreme precipitation in

mainland China. However, most of these studies examined the spatial-temporal variation and patterns, and disaster risk induced by extreme precipitation (You et al. 2011; Zhang et al. 2011a; Wang et al. 2013; Zhou et al. 2014; Yin et al. 2015; Wu and Huang 2015; Sun and Zhang 2017; Wang et al. 2017a; Gao et al. 2017). Studies of nonstationarity and spatial heterogeneity of extreme precipitation have been limited, and the spatial heterogeneity trend of the design rainstorm based on the nonstationary assumption and the continuous difference between the changing trend of the design rainstorm based on nonstationarity and stationarity assumptions remain poorly understood. A better understanding of these two concepts may allow China to better prepare for and defend against disasters induced by extreme precipitation.

Therefore, the objectives of this study were to (1) investigate the historical changing trend and spatial heterogeneity of the design rainstorm across mainland China with focus on the effect of potential nonstationarity and (2) explore the continuous difference of the changing trend of the design rainstorm based on nonstationary and stationary assumptions to calculate design rainstorm values. The results of this work should allow determination of the changing characteristic and law of extreme precipitation, providing great scientific and practical merits for hydraulic engineering construction, water resource and security management, and flood hazard prevention and reduction.

## 2 Data and methodology

### 2.1 Data

In this study, we used a high-resolution (0.5° × 0.5°) gridded daily precipitation data set (GPD) gathered from 2474 rain gauge stations distributed in mainland China from 1961 to 2013. Released by the National Meteorological Information Centre (NMIC) (NMIC, http://cdc.nmic.cn/home.do), this GPD data set has been validated so that each of the gridded box series is highly correlated with the original observational series with a small error and can therefore be used to characterize precipitation variability (NMIC 2012). Many studies have rigorously calibrated the data set, and the data have been verified to exhibit good applicability and rationality (Ren et al. 2015; Wu et al. 2016; Wang et al. 2017c; Lai et al. 2019). As shown in Fig. 1, there are a total of 3825 grid points across mainland China, and an individual grid point is the basic research unit of this study. Additionally, in our earlier research (Wang et al. 2017c), mainland China was divided into 50 homogeneous regions according to both the characteristics of mean annual precipitation and location indices using a fuzzy c-means method. This study applied the same 50 homogeneous regions to extend this research.

### 2.2 Extreme precipitation indices

Currently, there are three main kinds of methods to define extreme precipitation indices (Alexander et al. 2006; Zhang et al. 2011b): (a) precipitation exceeds a fixed threshold, such as if the daily precipitation exceeds 25 mm (Wu et al. 2016); (b) precipitation exceeds a variable threshold, for example, the 95th or 99th percentile (Bonsal et al. 2001); and (c) there is maximum precipitation within a specified period, such as yearly maximum consecutive 1-day (RX1DAY) or 5-day (RX5DAY) precipitation (Min et al. 2011).

This study used the design value of extreme precipitation (i.e., the design rainstorm value) to illustrate the spatial-temporal variance trend of extreme precipitation. The design rainstorm value was calculated by fitting an extreme value distribution function (e.g., generalized extreme value (GEV)) and computing a certain return period (such as a 100-year return period) value based on RX1DAY or RX5DAY series. This value is considered as an excellent indicator to measure precipitation extremes (Cooley et al. 2007; Pall et al. 2007). The two indices (RX1DAY and RX5DAY) are widely adopted in the design of water conservancy projects, with years of application worldwide (Min et al. 2011). These indices can better characterize extreme events and are widely utilized to estimate the extreme precipitation of a certain return period (such as 100-year return level values). In this study, the design rainstorm values (20-, 50-, and 100-year return periods) were generated by fitting the GEV distribution with the RX1DAY or RX5DAY series data.

### 2.3 Design rainstorm trend analysis

#### 2.3.1 GEV

The GEV distribution is based on extreme value theory and block maxima theory with three parameters, and is widely adopted to quantify the intensity and frequency of extreme precipitation. Compared to other distributions, it is more appropriate to estimate precipitation frequency (Svensson and Jones 2010). The distribution function of GEV is as follows:

$$F(x) = \begin{cases} \exp\left[-(1+kz)^{-\frac{1}{k}}\right], k \neq 0 \\ \exp[-\exp(z)], k = 0 \end{cases} \quad (1)$$

where $z = \frac{x-\mu}{\sigma}$; $\mu$, $\sigma$, and $k$ are the location, scale, and shape parameters, respectively. The shape parameter $k$ determines whether the distribution has an upper bound. Specific GEV distributions are defined by the value of $k$. The Gumbel distribution exists when $k = 0$, $k < 0$ implies a Frechet distribution, and $k > 0$ indicates a Weibull distribution (Asl et al. 2013).

In this study, the quantification of design rainstorm values (e.g., 20-, 50-, and 100-year return periods) was based on the annual maximum method and the GEV distribution. The

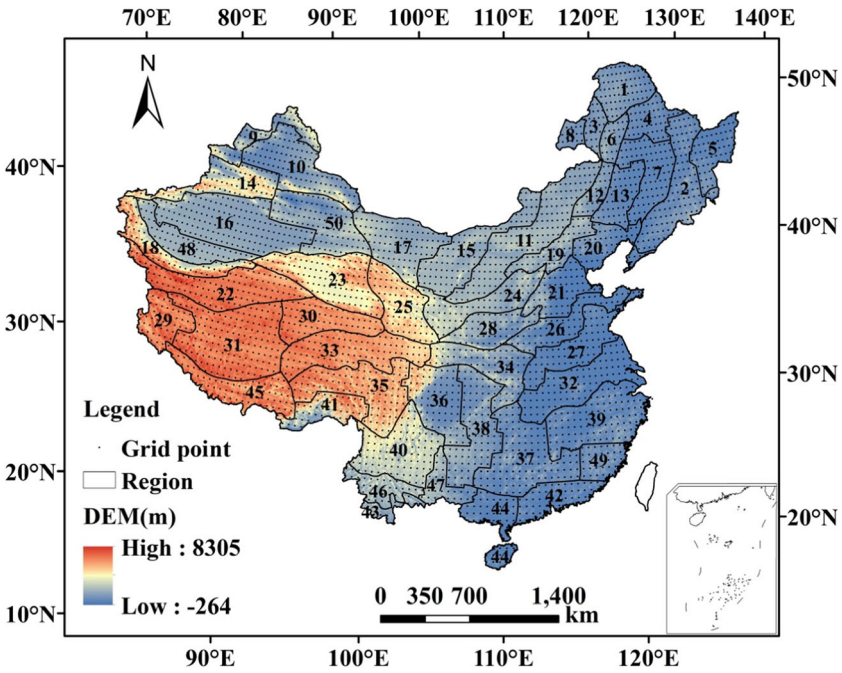


**Fig. 1** Spatial distribution of 3825 grid points and the 50 homogeneous regions across mainland China. The Arabic numerals in each region represent the serial number of the homogeneous region

annual maximum method was used to extract the annual maximum precipitation series (AMP, such as the RX1DAY and RX5DAY series) from the daily precipitation series. Then, the GEV parameters were estimated by the AMP series with the maximum likelihood estimation (MLE) method, allowing different design rainstorm values to be calculated. This method of using AMP series data to calculate the design rainstorm values is commonly applied to hydraulic engineering design (Bonnin et al. 2004).

### 2.3.2 The 30-year moving window

The frequency analysis using GEV is based on the stationary assumption, which means the AMP series used to estimate GEV parameters is stationary (Chow et al. 1988). As described above, the stationarity may be disturbed due to climate change. Instead of using the whole AMP series to estimate the GEV parameters as is done in most studies, some studies have used a fixed-year moving window method to address potential nonstationary effects, such as a 30-year (Kao and Ganguly 2011; Ghosh et al. 2012) or 51-year (Kharin and Zwiers 2005) moving window method. The 30-year moving window method (30YM) is more widely used to investigate historical changing trends and spatial heterogeneity because it requires a shorter time series. Additionally, the 30-year standard can provide higher confidence for low-frequency extremes than the 20-year standard previously proposed by the World Climate Research Program's (WCRP's) Coupled Model Intercomparison Project Phase 3 (CMIP3) (Kharin et al. 2007). Moreover, according to the World Meteorological Organization (WMO) (http://www.wmo.int/pages/prog/wcp/ccl/faqs.php), the classical period of climate is defined as 30 years. Therefore, considering the effects of potential nonstationarity, we used 30YM to investigate the historical continuous changing trend and the spatial variability trend of the design rainstorm for mainland China from 1961 to 2013.

For a total of AMP series (i.e., RX1DAY and RX5DAY in this study), $X = \{X_1, X_2, \cdots X_i, \ldots, X_n\} (0 < i < n \,\&\, i \in N^+)$, where $n$ is the total length of the series, $X_i$ is the AMP of the $i^{\text{th}}$ year, and $N^+$ represents the natural number set.

For 30YM, a total of $(n-29)$ of AMP sub-series with a fixed temporal length of 30 years can be obtained:

$$\{T_1, T_2, \ldots, T_j \ldots, T_{n-29}\} \quad (0 < j < n-29 \& j \in N^+) \tag{2}$$

where $T_j$ can be expressed as

$$T_j = \{X_j, X_{j+1} \ldots, X_{j+29}\} \quad (0 < j < n-29 \& j \in N^+) \tag{3}$$

In this study, the total length of the series is 53 years (1961–2013, $n = 53$) and the number of the sub-series in both 30YM and 30YBI is 24 (i.e., $n-29 = 24$). The sub-series of $T_j$ is utilized to estimate the GEV parameters (i.e., $\mu$, $\sigma$, and $k$) based on the MLE method (a detailed estimation of GEV parameters in 30YM and 30YBI is shown in Supplementary File), and the return period value $y_i^T$ related to a $T$-year return period is calculated from the function of GEV according to Eq. (1):

$$y_i^T = \begin{cases} u - \dfrac{k}{\sigma}\left\{1 - \left[-\ln\left(1-\dfrac{1}{T}\right)\right]^{-k}\right\}, k \neq 0 \\ u - \sigma \ln\left[-\ln\left(1-\dfrac{1}{T}\right)\right], k = 0 \end{cases} \tag{4}$$

Based on 30YM, the design rainstorm value series of different return periods can then be arranged in chronological order and can be described as

$$y^T = \left\{y_1^T, y_2^T, \ldots, y_{n-29}^T\right\} \tag{5}$$

In addition to applying the 30YM, this study also created a new method called the 30-year-based increasing window method (30YBI) to analyze the differences between nonstationary and stationary assumptions when calculating the design rainstorm values and the continuously changing trends of extreme precipitation. The 30YBI, since 1990, differs from 30YM which always uses the most recent 30-year AMP series (ignoring the AMP sub-series from more than 30 years ago). Instead, the 30YBI always adopts all available historical AMP series (from 1961 to that year) for each year. Details of 30YBI are presented in the Supplementary File. According to the extreme value theory, the series utilized to estimate GEV distribution should be in accordance with the stationary assumption. Thus, 30YM indicated that the latest 30-year series is in accordance with the stationary assumption, and 30YBI indicated that the whole series was stationary. Therefore, 30YM has weakened the influence of potential nonstationarity to some degree.

#### 2.3.3 Linear regression method

Linear regression is utilized to illustrate the temporal trend of design rainstorm values and their spatial variance (i.e., quantification of spatial heterogeneity) as calculated from GEV estimation. The linear regression equation is as follows:

$$\hat{y} = \hat{a} + \hat{b}x \tag{6}$$

$$\hat{b} = \frac{\sum_{i=1}^{n}\left(x_i - \bar{x}\right)\left(y_i - \bar{y}\right)}{\sum_{i=1}^{n}\left(x_i - \bar{x}\right)^2} \tag{7}$$

$$\hat{a} = \bar{y} - \hat{b}x \tag{8}$$

where $\hat{a}$ is the intercept and $\hat{b}$ represents the slope; $x$ is the independent variable (time) and $y$ is the dependent variable (precipitation depth or its spatial variance); $x_i$ represents the $i^{\text{th}}$ year and $\bar{x}$ is the arithmetic mean of $x_i$; $y_i$ represents the precipitation depth of $i^{\text{th}}$ year and $\bar{y}$ is the arithmetic average of $y_i$.

The temporal trend and spatial variance trend of the design rainstorm based on the series (Eq. (5)) can be calculated according to Eq. (7), and the slope can be expressed as

$$\hat{b}^T = \frac{\sum_{j=1}^{n-29}\left(x_j - \bar{x}\right)\left(y_j^T - \overline{y^T}\right)}{\sum_{j=1}^{n-29}\left(x_j - \bar{x}\right)^2} \tag{9}$$

### 2.4 Uncertainty analysis

The main sources of uncertainty of design rainstorm values include the goodness of fit of the GEV distribution and the uncertainty in the estimation of GEV parameters. For the goodness-of-fit test for GEV distribution, this study adopted the Kolmogorov-Smirnov (KS) test, and an empirical distribution was considered fitted if the significance of the KS test was lower than 1% (Kao and Ganguly 2011; Ghosh et al. 2012).

To study the uncertainty of estimated GEV parameters, given the relatively limited number of samples from each 30YM window on each grid point, a 1000-member bootstrapping method (Efron and Tibshirani 1994; Johnson 2001) was adopted. Among the 1000 members, bootstrapping was performed by randomly sampling 30 times from each 30YM series with replacement. In this way, 1000 groups of sub-series can be obtained and each sub-series includes 30 values. Next, each group of sub-series can be utilized to fit the GEV distribution and the 1000 groups of values of the design rainstorm and the GEV parameters can be finally acquired. The uncertainty of the design rainstorm values based on the 1000-member bootstrapping at each 30YM can be calculated as

$$U = \frac{\left(R_{90} - R_{10}\right)}{R_{50}} \times 100\% \tag{10}$$

where $U$ is the quantized value of uncertainty, where a bigger value corresponds to greater uncertainty; $R_{90}$, $R_{10}$, and $R_{50}$ are the 90th, 10th, and 50th percentiles of the 1000 groups of design rainstorm values, respectively.

## 3 Results and analysis

### 3.1 Trend analysis of AMP based on the 30-year moving average

Based on the 53-year AMP (RX1DAY and RX5DAY) series, the successive 30-year moving average trend and 30-year moving variance trend of mainland China were determined and are shown in Fig. 2. Both the trend lines and their 95% confidence bounds of the 30-year moving average (Fig. 2 a and c) and 30-year moving temporal variance (Fig. 2 b and d) show an increasing trend for both the RX1DAY and RX5DAY data. In detail, the trend line shows that the 30-year moving average values increased about 0.48 mm/decade (RX1DAY) or 0.55 mm/decade (RX5DAY) over recent decades. These significant growing trends indicate significantly intensified extreme precipitation and enhanced interannual difference for mainland China during 1961–2013. Similar temporal trends of extreme precipitation were also reported in a related

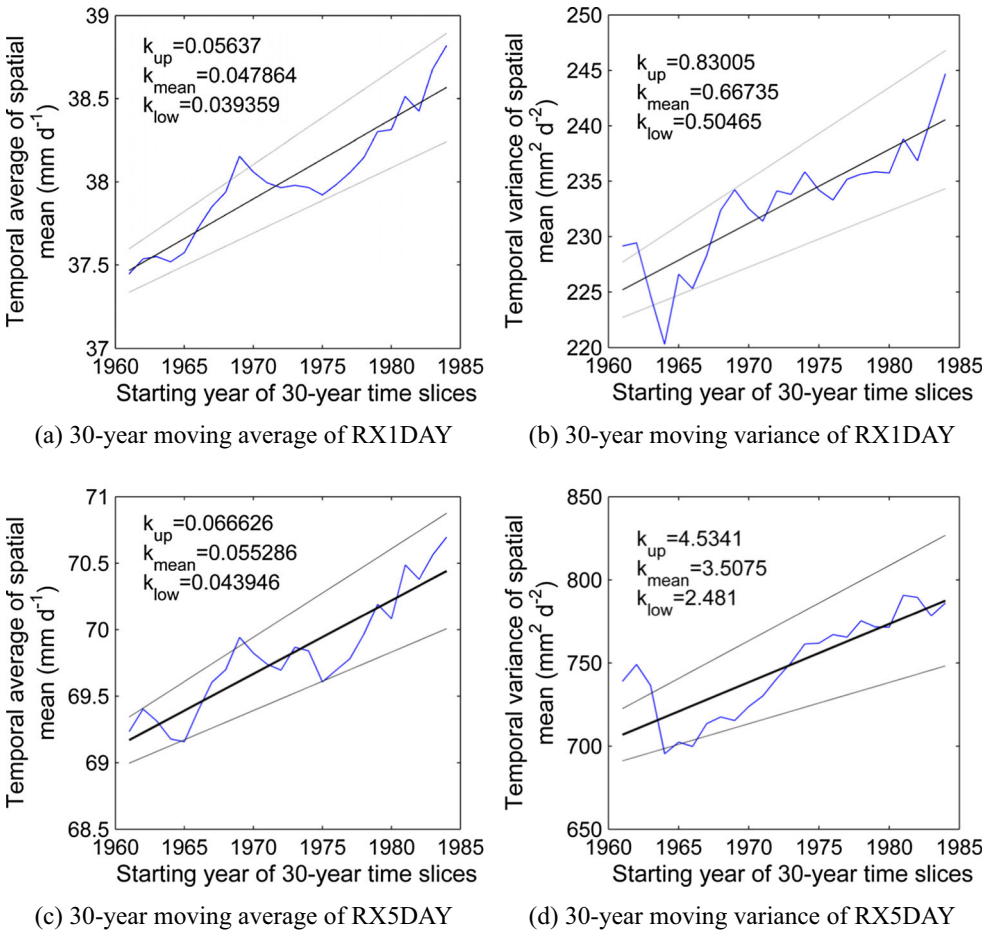


(a) 30-year moving average of RX1DAY (b) 30-year moving variance of RX1DAY

(c) 30-year moving average of RX5DAY (d) 30-year moving variance of RX5DAY

**Fig. 2** The successive 30-year moving average trend and 30-year moving variance trend of mainland China. The bold solid straight lines are the trend lines; the fuzzy solid straight lines are their bounds (5% significance level); $k_{mean}$, $k_{up}$, and $k_{low}$ represent the slope of trend lines, upper bounds, and lower bounds, respectively; similarly hereinafter

study conducted by Sun et al. (2017b), supporting the rationality of these results. However, whether the intensified AMP together with the increasing interannual difference suggests that the design rainstorm has changed requires further investigation by exploring the changing trend and spatial heterogeneity of the design rainstorm.

### 3.2 Variation of design rainstorm on the national and gridded scale

The temporal trend of the design rainstorm values (20-, 50-, and 100-year period) for each grid point is shown in Fig. 3 and Fig. S1. The temporal trend of the design rainstorm values showed no spatially uniform or coherent trends in 30YM. However, some grid points with the same positive or negative trend implied occasional spatial coherence (especially for the RX5DAY data). Specifically, in southeast and northeast China, the majority of grid points showed increasing trends with high growth rates, other increasing trends with lower growth rates were mainly distributed in the west and northwest China, and the grid points with rapid decreasing trends were mainly found in southwest and central China, as well as the southern coastal area.

According to the statistical percentage of the design rainstorm trend over all grid points (Fig. 4), approximately 75% of the grid points showed significant trends (including significant increasing or decreasing trend, at the 5% significance level). Among the grid points across mainland China, the significant increasing trends were dominant (more than 40%), and approximately one-third of grid points presented significant decreasing trends. Although their spatial distributions presented diverse characteristics, most grid points of mainland China showed statistically significant trends with homogeneity observed in local regions (e.g., southeast, northeast, and southwest China).

The temporal trends of the national scale design rainstorm values based on 30YM are shown in Fig. 5 and Fig. S2. The trend of the 30YM design rainstorm values and their spatial variance both were significantly increasing (5% significance level). In detail, the trend lines show that the design rainstorm values increased about 0.84–1.25 mm/decade (20-, 50-, and 100-year return periods of RX1DAY) and 1.52–2.82 mm/decade (20-, 50-, and 100-year return periods of RX5DAY) over the 24 years. Due to the neutralization of increasing and decreasing trends, these changes seem somewhat negligible at the national average level, but the trends in many grid points

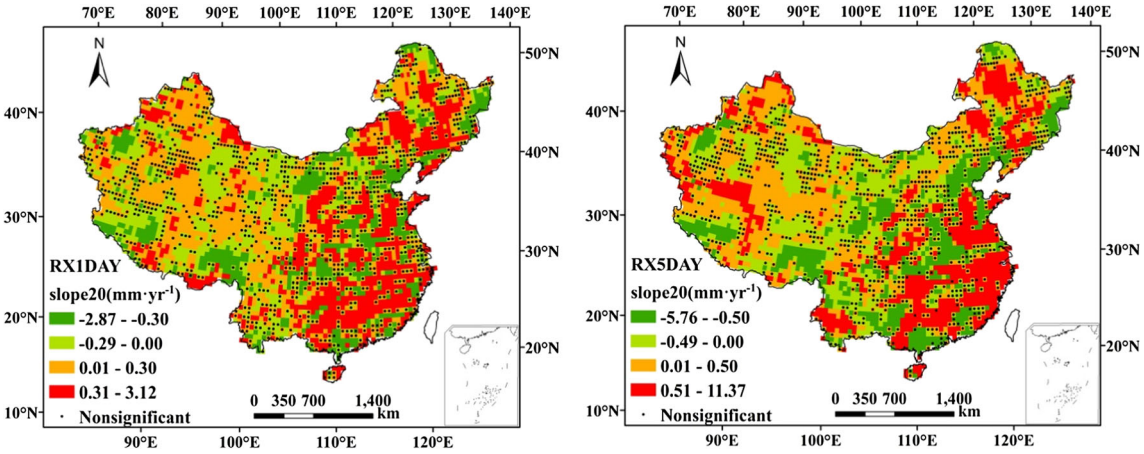


**Fig. 3** Spatial distribution of 30YM temporal trends of design rainstorm (20-year return period) on gridded scale. Black solid dots represent the grid points that fail to pass the 5% significance test

with high nonstationarity show even more than 3–8 mm/decade (20-, 50-, and 100-year return periods of RX1DAY) and 5–10 mm/decade (20-, 50-, and 100-year return periods of RX5DAY). The significant growing trends suggest that significantly intensified design rainstorm and enhanced spatial heterogeneity can be observed, indicating that the increasing risk of suffering heavy extreme rainfall, flooding, and drought events may show geographic diversity across mainland China.

### 3.3 Spatial heterogeneity of the design rainstorm on the regional scale

The 30YM spatial (regional) variance trends of design rainstorm values in different homogeneous regions (Wang et al. 2017c) were determined and are shown in Fig. 6 and Supplementary File (Fig. S3 and Table S1). Other than a few regions showing no statistically significant trend, most regions presented either a positive or negative trend (5% significance level).

Generally, more regions showed a positive trend (especially for RX1DAY) than negative ones, which is similar to the results of Fig. 5 and Fig. S2. Regions in the southeast, northeast, and northwest China were mainly dominated by a positive trend, suggesting enhanced spatial heterogeneity over the last decades, and regions in southwest and western China mainly showed a negative trend, indicating decreasing spatial heterogeneity. Some regions (e.g., regions 37 and 26) presented significantly increasing intensity and spatial variance, and these changes may cause more extreme rainfall depth. Decreasing intensity and spatial variance were significantly observed in local regions (e.g., region 20), implying lower flooding risk and fewer impacted areas. Some regions (e.g., region 38) exhibited increasing intensity but decreasing spatial

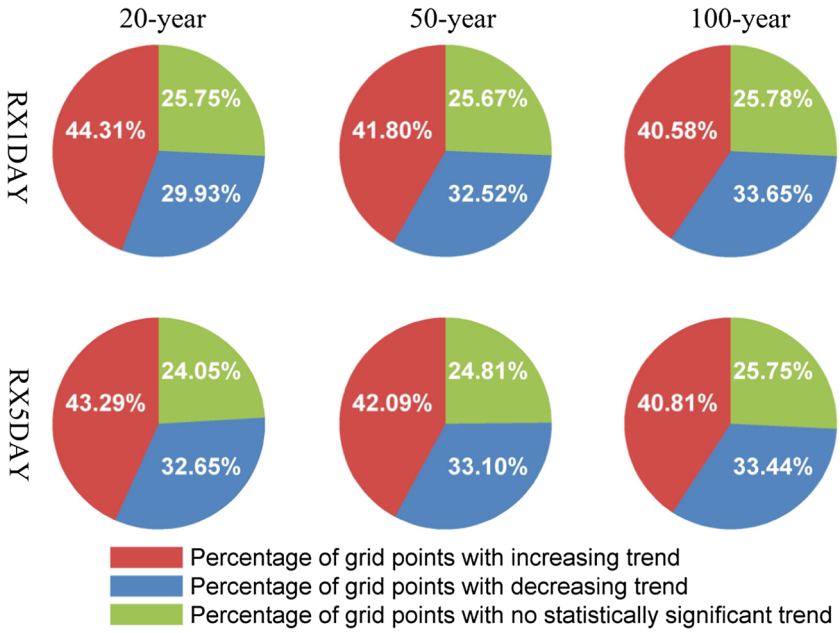


**Fig. 4** Statistical percentages (95%) of 30YM temporal trends of design rainstorm in 5% significance level

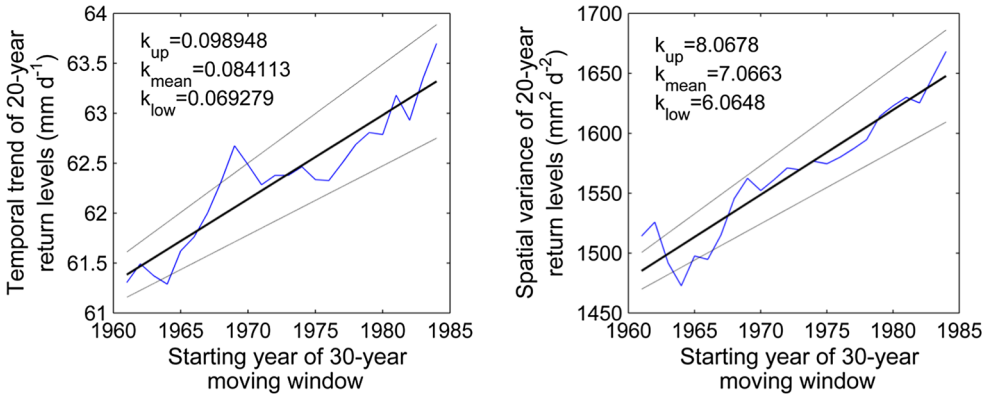


(a) RX1DAY

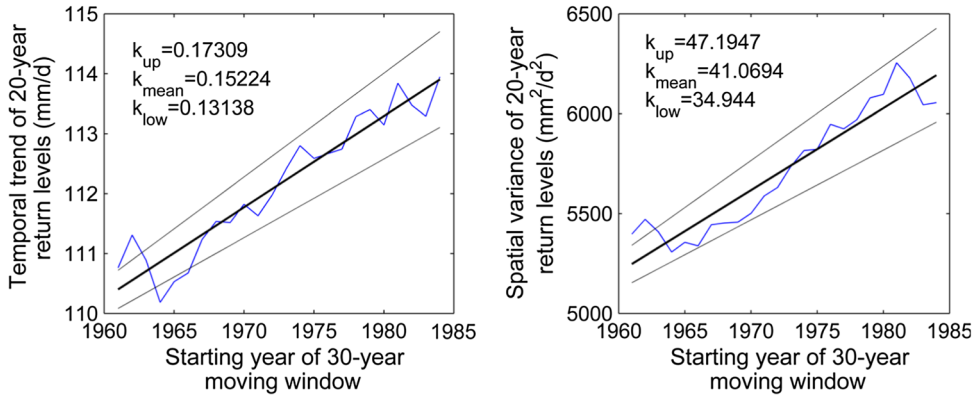


(b) RX5DAY

**Fig. 5** Temporal trends and spatial variance trends of design rainstorm (20-year return period) on a national scale

variance, which may lead to heavy droughts or flood disasters becoming more homogenously widespread (Liu et al. 2015).

Accordingly, we can see that not only the intensity of extreme precipitation but also the spatial variation can directly influence the determination of the design rainstorm standard. Ignoring spatial variation and the use of a single design standard may not be appropriate for some particular sub-regions located within a homogeneous region. Overall, spatial variation is a significant concern even in some homogeneous regions where the intensity and spatial heterogeneity of extreme precipitation show obviously enhanced trends.

### 3.4 Uncertainty analysis for design rainstorm values

A total of 1000 bootstrapping iterations were conducted for each 30-year window to explore the uncertainties and

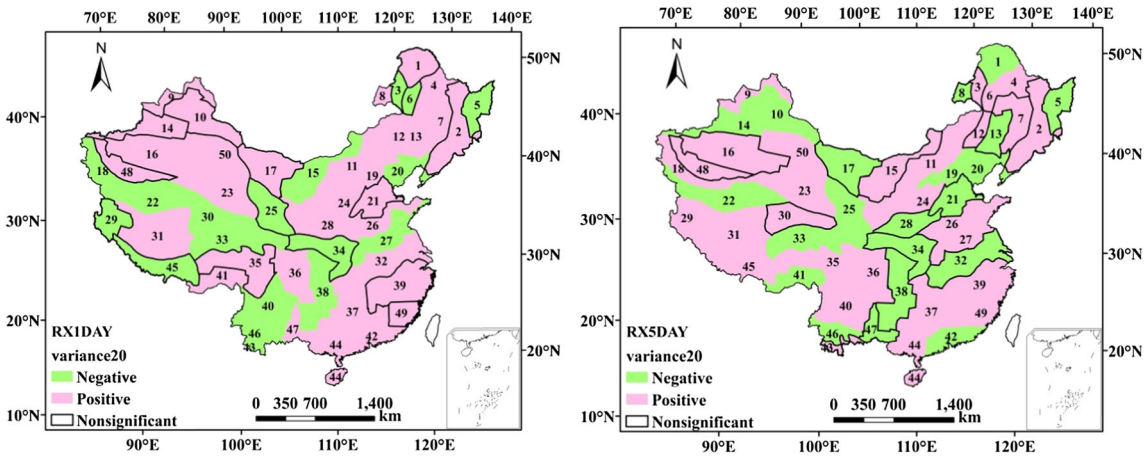


**Fig. 6** Spatial distribution of 30YM spatial variance trends of design rainstorm (20-year return period) on a regional scale. The regions failing to pass the 5% significance test are labeled by the bold polylines

their spatial distribution of design rainstorm values across mainland China. This study utilized three representative 30-year windows (i.e., 20-, 50-, and 100-year return periods) to analyze the spatial distribution of uncertainty, and the results are shown in Fig. 7 and the Supplementary File (Fig. S7, Fig. S8, and Fig. S9). Generally, the quantized values of uncertainty (the *U* values) of the three return periods posed similar spatial distribution characteristics. The *U* values in northwest China were generally larger than the values of other regions, and the smallest *U* values were generally detected in southwest regions, implying an increasing trend from south to northwest China. Taking the 20-year return period as an example (Fig. 7 and Fig. S7), the *U* values in most grid points were less than 30% (especially in southwest and southern China). However, the grid points with large *U* values were mainly concentrated in northwest China, and most *U* values exceeded 50%. In addition, we found that the *U* values showed an increasing trend as the return period increased from a 20-year to 100-year period, similar to the findings of Zhu et al. (2016).

In most of China, it is reasonable to use the GEV distribution in frequency analysis and to calculate design rainstorm values with large return periods (i.e., 20-, 50, and 100-year in this study) based on AMP series generated by the annual maximum method. However, calculating large return periods of design rainstorm results in great uncertainties for all of mainland China, especially in northwest China where much greater uncertainties will occur even if a small return period was calculated. This phenomenon can likely be explained by two factors: the AMP values in northwest China are relatively small, and the AMP series for the 30-year analysis may not be sufficiently long for the high return period. Accordingly, the uncertainty analysis method including 1000 bootstrapping iterations can identify potential uncertainty.

## 4 Discussion

### 4.1 Comparison of results with those from other studies

We observed significantly increasing intensity and an increasing spatial heterogeneity trend of the design rainstorm on a national scale. Additionally, even in geographically neighboring regions and grid points (Fig. 3, Fig. S1, Fig. 6, and Fig. S3), the spatial distribution of temporal trend showed no statistically significant spatial uniformity, although occasional spatial coherence was observed. Generally, the increasing trends of intensity and spatial heterogeneity of the design rainstorm were significant across mainland China. These characteristics are similar to those of another large country, India, which lacks uniform trends and exhibits increasing spatial variability (Ghosh et al. 2012), suggesting that the spatial characteristic of heterogeneity of extreme precipitation may be more obvious in larger countries.

We looked at southwest China (SW, including Yunnan, Guangxi, and Guizhou provinces) to further verify the reasonability of these results. The spatial distribution of the 30YM temporal trend of intensity (e.g., 100-year return period of RX5DAY) was determined and is shown in Fig. S4. Obviously, except a few scattered grid points, nearly all the grid points exhibited a significant trend. The southwest of Yunnan and the northeast and southwest of Guangxi were more likely to exhibit a significant increasing trend, meaning increased intensity and frequency of extreme precipitation in these areas in recent decades. Significant decreasing trends were widespread in the middle and north parts of the SW, indicating decreased intensity and frequency of extreme precipitation during 1961–2013. Generally, this spatial distribution of changing trend in southwest China was extremely similar to the findings reported by Liu et al. (2015), who found that atmospheric circulations led to such characteristics of extreme precipitation.

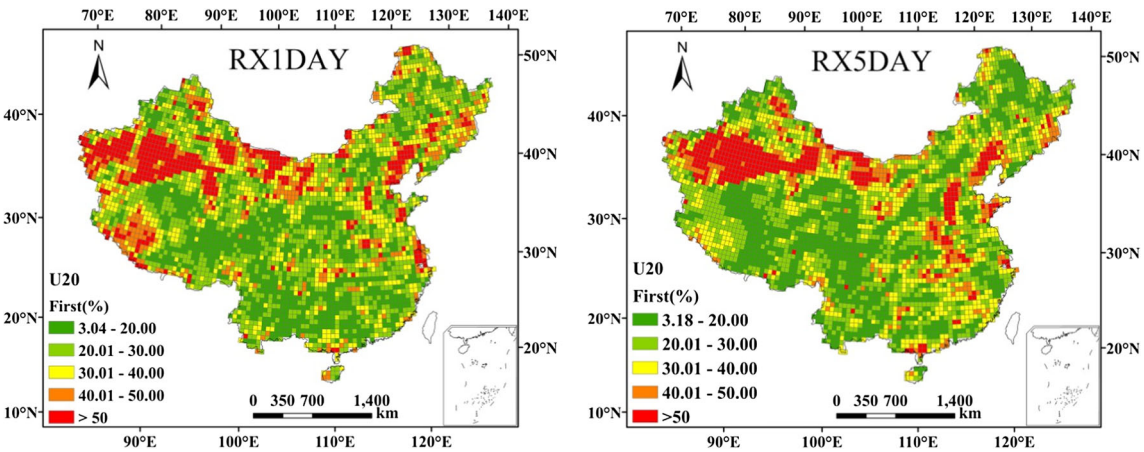


**Fig. 7** Spatial distribution of *U* values (20-year return period) in the first (1961–1990) 30-year window

### 4.2 Spatial distribution of design rainstorm trend based on 30YBI

The spatial distribution of 30YBI temporal trends of design rainstorm across mainland China is shown in Fig. 8 and Fig. S5, and the statistical percentages of 30YBI temporal trends are summarized in Fig. S6.

Figure 8 and Fig. S5 show that the spatial distribution of the 30YBI temporal trends showed no statistically significant spatial uniformity. In detail, in the south, east, and northeast China, increasing trends are more likely to be observed, meaning that intensified design rainstorm appeared based on the stationarity assumption. An obvious decreasing trend can be mainly observed in southwest and north China, indicating that the design rainstorm shows a decreasing trend based on the stationarity assumption. These spatial distribution characteristics were extremely similar to those for 30YM, but with smaller absolute values of the maximal and minimal trends in 30YBI than those in 30YM, suggesting that the 30YBI method somewhat underestimates the impact of nonstationarity.

According to the statistical percentage of design rainstorm trend in 30YBI (Fig. S6), a majority of grid points (more than 75% grid points) showed significant trends (at the 5% significance level). The percentage with significant increasing trend became approximately equal to that with decreasing trend, which indicates that some grid points showed an increasing trend in 30YM but showed a decreasing trend in 30YBI. Overall, it is adverse to the accurate and effective design of water conservancy projects to underestimate nonstationarity.

### 4.3 Calculation differences of design rainstorm values by applying stationarity and nonstationarity assumptions

To further analyze the difference in the calculation of design rainstorm values based on nonstationarity and stationarity assumptions, all the grid points in mainland China were divided into six classes according to the given standard (Fig. 9). The spatial distributions for the classes are displayed in Fig. 10 and Fig. S10.

According to the data presented in Fig. 9, Fig. 10, and Fig. S10, over 85% of the grid points (involving four classes) showed similar characteristics both in 30YM and 30YBI, and can be classified as |30YM+|>|30YBI+|, |30YM+|<|30YBI+|, |30YM−|>|30YBI−|, and |30YM−|<|30YBI−|. However, the grid points in the four classes have a common feature in that the absolute values of trends in 30YM were generally larger than those in 30YBI, which may be because the percentage of |30YM+|>|30YBI+| (over 40%) was much larger than that of |30YM+|<|30YBI+| (less than 6%), and the percentage of |30YM−|>|30YBI−| (over 30%) was also much larger than that of |30YM−|<|30YBI−| (approximately 8%). The remaining two classes (i.e., (30YM+) and (30YBI−), (30YM−) and (30YBI+)) were approximately 15% or lower, and showed opposite trends between 30YM and 30YBI. This means that the difference (the absolute value of 30YM and 30YBI) of the design rainstorm values based on nonstationarity and stationarity assumptions may increase year by year.

For water conservancy project design based on historical rainfall data, if the actual design rainstorm values underestimate the impacts of historical nonstationarity and are lower than the expected design rainstorm values, there may be an increased risk of heavy extreme flood events. In particular, the three classes (i.e., |30YM+|>|30YBI+|, |30YM−|<|30YBI−|, and (30YM+) and (30YBI−)) should be carefully considered because they would become more dangerous with time. For the class |30YM+|>|30YBI+| (over 40%), the absolute value of the increasing trend based on the stationarity assumption was lower than that based on the nonstationarity assumption, causing underestimation of the design rainstorm. For the class |30YM−|<|30YBI−| (approximately 8%), although the points

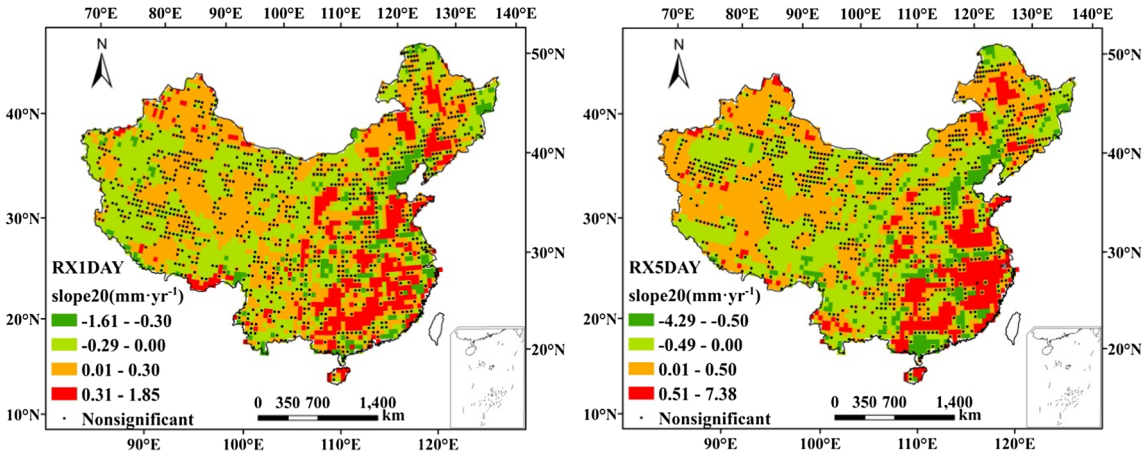


**Fig. 8** Spatial distribution of 30YBI temporal trends of design rainstorm (20-year return period) on a gridded scale. The black solid dots represent the grid points without passing the 5% significance test

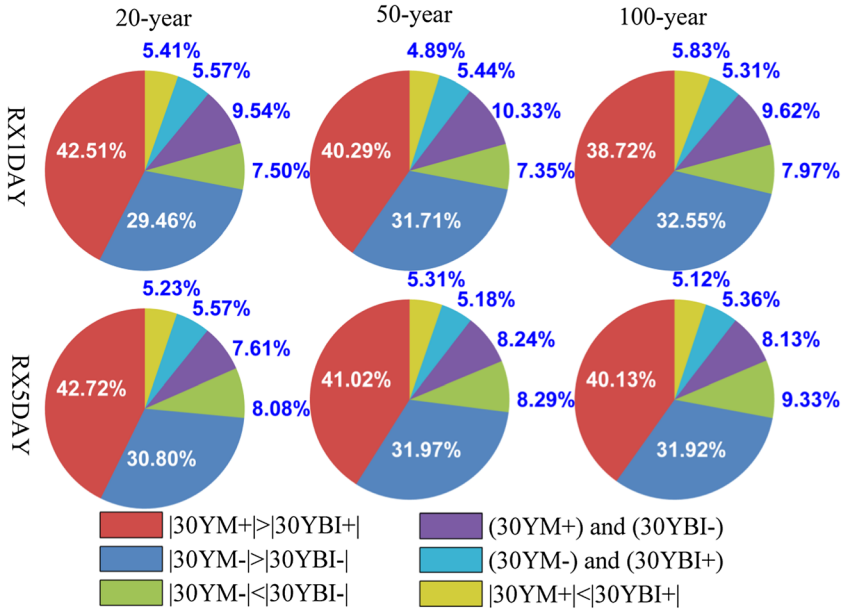


**Fig. 9** Statistical percentage of temporal trend of different classes. According to the positive or negative of temporal trend in both 30YM and 30YBI methods, all the grid points are divided into six classes: (1) grid points showed increasing trend in both 30YM and 30YBI method while the absolute value of 30YM trend was larger (i.e., |30YM+|>|30YBI+|); (2) grid points showed increasing trend in both 30YM and 30YBI while the absolute value of 30YBI trend was larger (i.e., |30YM+|<|30YBI+|); (3) grid points showed decreasing trend in both 30YM and 30YBI while the absolute value of 30YM trend was larger (i.e., |30YM−|>|30YBI−|); (4) grid points showed decreasing trend in both 30YM and 30YBI while the absolute value of 30YBI trend was larger (i.e., |30YM−|<|30YBI−|); (5) grid points showed increasing trend in 30YM but showed decreasing trend in 30YBI (i.e., (30YM+) and (30YBI−)); (6) grid points showed decreasing trend in 30YM but showed increasing trend in 30YBI (i.e., (30YM−) and (30YBI+)). The symbols "+" and "−" represent the increasing and decreasing trends, respectively

in both 30YM and 30YBI presented decreasing trends, the decreasing trend based on the stationarity assumption was more significant than that based on the nonstationarity assumption, leading to a larger reduction and the underestimation of the design rainstorm in 30YBI. For the class (30YM+) and (30YBI−) (approximately 8~10%), unlike the increasing trend based on the nonstationarity assumption, there was a decreasing trend based on the stationarity assumption, which may underestimate the design rainstorm. Overall, the design rainstorm of approximately 57% grid points may be underestimated in 30YBI (stationarity assumption), and these grid points were mainly distributed in southeastern, northeastern, and western China (Fig. 10 and Fig. S10).

From the 50 homogeneous regions (Fig. 1), we can examine region 12 (northeast of mainland China) as an example. The design rainstorm values of the 20-, 50-, and 100-year return periods (RX1DAY) in the first 30YM and 30YBI window (the first 30-year window) were 59.3, 68.3, and 75.2 mm, respectively, and the design storm values based on the last 30YM window were 71.6, 91.4, and 109.3 mm, respectively. The results of 30YM were significantly larger than those of 30YBI (65.4 mm, 79.3 mm, and 90.8 mm), and the increase

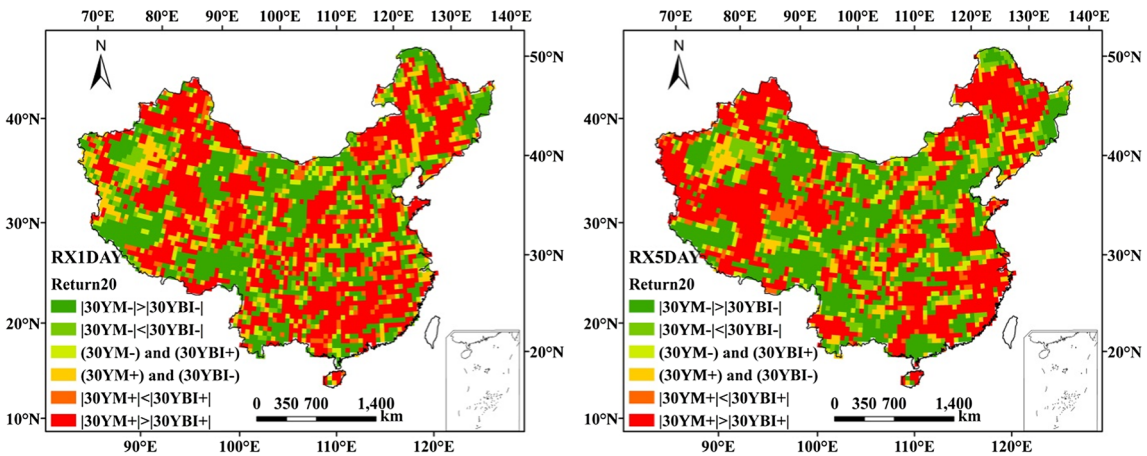


**Fig. 10** Spatial distribution of temporal trend of design rainstorm (20-year return period) and classes

rates respectively reached 9.4%, 15.3%, and 20.4%. Subregions 8, 50, and 7 had increasing rates that were more than 6% (20-year), 8% (50-year), and 10% (100-year). In terms of the capability to limit the effects of rare extreme precipitation events, the infrastructure of water conservancy projects designed during 1961–2013 may not be sufficient in these regions.

Accordingly, for regions with significant increasing trends, the use of the entire precipitation series to determine the design of hydraulic engineering may cause the actual design standard to be lower than the expected design standard. However, if the increasing historical trend continues in the future, the capability of old infrastructure to resist rare extreme precipitation events would also decrease year by year. For these structures (e.g., key water control projects), the regional precision of real-time prediction for extreme precipitation and flooding events should be improved, and the plans for reservoir regulation, river and lake control, and water sources management should be optimized to reduce the probability of floods induced by the ultra-expected extreme precipitation events.

Given the differences between using the most recent precipitation sub-series and using the entire precipitation series, we can see that the use of the most recent sub-series (e.g., 30YM) to compute the design rainstorm values may decrease the potential nonstationarity problem more than the use of the entire precipitation series (e.g., 30YBI), especially in regions that exhibit increasing trends of intensity and frequency of extreme precipitation. Accordingly, it may imply that the method that uses the most recent sub-series (e.g., 30YM) to calculate the design rainstorm values in southeastern, northeastern, and western China may better guarantee the safety of infrastructure.

## 5 Conclusions

This study investigated the historical changing trends and spatial heterogeneity of the design rainstorm with a focus on the effects of potential nonstationarity and stationarity assumptions. The conclusions can be summarized as follows:

(a) For the changing trend of the design rainstorm in 30YM, a significant increasing intensity of the design rainstorm can be detected on the national scale. For the gridded and regional scale, the distribution of the design rainstorm changing trend showed no spatial uniformity: the south, east, and northeast parts of China are dominated by a significant intensified trend and the southwest and north parts of China showed a decreasing trend. Additionally, the calculation of the design rainstorm value in northwest China showed large uncertainty. Generally, the calculation of the design rainstorm value presented large uncertainty across mainland China when utilizing a large return period of the design rainstorm.

(b) In 30YM, the spatial variance trend showed a significant increasing trend on the national scale, indicating an increasing spatial heterogeneity of the design rainstorm. On the regional scale, southeast, north, northeast, and northwest China mainly presented an increasing trend and southwest and west China showed a decreasing trend, indicating that spatial heterogeneity has great regional differentiation. This heterogeneity should be considered when designing the infrastructure of a water conservancy project, formulating water resource management policies, and preventing and mitigating disaster.

(c) The spatial distribution of temporal trends in 30YBI showed similar characteristics to that in 30YM, but the design rainstorm values in 30YBI somewhat underestimated the impacts of nonstationarity. Adopting the design rainstorm value calculated by the most recent precipitation sub-series data (e.g., 30YM) would be a more reasonable strategy for most areas of mainland China, especially in southeastern, northeastern, and western China.

**Funding information** The research is financially supported by the National Key R&D Program of China (2018YFC1508201) and the National Natural Science Foundation of China (Grant Nos. 51879107, 51709117, 51579105, 91547202).

## References

Alexander LV, Zhang X, Peterson TC, Caesar J, Gleason B, Klein Tank AMG, Haylock M, Collins D, Trewin B, Rahimzadeh F, Tagipour A, Rupa Kumar K, Revadekar J, Griffiths G, Vincent L, Stephenson DB, Burn J, Aguilar E, Brunet M, Taylor M, New M, Zhai P, Rusticucci M, Vazquez-Aguirre JL (2006) Global observed changes in daily climate extremes of temperature and precipitation. J Geophys Res Atmos 111 (D5)

Asl SJ, Khorshiddoust AM, Dinpashoh Y, Sarafrouzeh F (2013) Frequency analysis of climate extreme events in Zanjan, Iran. Stochastic Environ Res Risk Assess 27(7):1637–1650

Bao J, Sherwood SC, Alexander LV, Evans JP (2017) Future increases in extreme precipitation exceed observed scaling rates. Nat Clim Chang 7(2):128–132

Bonnin GM, Todd D, Lin B, Parzybok T, Yekta M, Riley D (2004) Statistics of recent updates to NOAA/NWS rainfall frequency atlases. ASCE/EWRI World Water and Environmental Resources Congress, Salt Lake City, Utah

Bonsal BR, Zhang X, Vincent LA, Hogg WD (2001) Characteristics of daily and extreme temperatures over Canada. J Clim 14(9):1959–1976

Burt TP, Howden NJK, Worrall F (2016) The changing water cycle: hydroclimatic extremes in the british isles. Wiley Interdiscip Rev Water 3(6):854–870

Cancelliere A (2017) Non stationary analysis of extreme events. Water Resour Manag 31(10):3097–3110

Choi W, Tareghian R, Choi J, Hwang C (2014) Geographically heterogeneous temporal trends of extreme precipitation in Wisconsin, USA, during 1950–2006. Int J Climatol 34(9):2841–2852

Chow VT, Mainment DR, Mays LW (1988) Applied hydrology. McGraw-Hill, New York

Cong Z, Yang D, Gao B, Yang H, Hu H (2009) Hydrological trend analysis in the Yellow River Basin using a distributed hydrological model. Water Resour Res 45(7):335–345

Cooley D, Nychka D, Naveau P (2007) Bayesian spatial modeling of extreme precipitation return levels. J Am Stat Assoc 102(479): 824–840

Dai L, Van Rijswick HFMW, Driessen PPJ, Keessen AM (2017) Governance of the sponge city programme in China with Wuhan as a case study. Int J Water Resour Dev 12:1–19

Donat MG, Lowry AL, Alexander LV, O'Gorman PA, Maher N (2017) More extreme precipitation in the world's dry and wet regions. Nat Clim Chang 7(2):154–158

Du T, Xiong L, Xu CY, Gippel CJ, Guo S, Liu P (2015) Return period and risk analysis of nonstationary low-flow series under climate change. J Hydrol 527:234–250

Efron B, Tibshirani RJ (1994) An introduction to the bootstrap. CRC Press, Boca Raton, Fla

Evans JP, Argueso D, Olson R, Luca AD (2017) Bias-corrected regional climate projections of extreme rainfall in south-east Australia. Theor Appl Climatol 130(3–4):1085–1098

Fischer EM, Knutti R (2016) Observed heavy precipitation increase confirms theory and early models. Nat Clim Chang 6(11):986–991

Gao T, Wang HJ, Zhou T (2017) Changes of extreme precipitation and nonlinear influence of climate variables over monsoon region in China. Atmos Res 197:379–389

Ghosh S, Das D, Kao SC, Ganguly AR (2012) Lack of uniform trends but increasing spatial variability in observed indian rainfall extremes. Nat Clim Chang 2(2):86–91

Goswami BN, Venugopal V, Sengupta D, Madhusoodanan MS, Xavier PK (2006) Increasing trend of extreme rain events over India in a warming environment. Science 314(5804):1442–1445

Gu X, Zhang Q, Singh VP, Chen X, Liu L (2016) Nonstationarity in the occurrence rate of floods in the Tarim River Basin, China, and related impacts of climate indices. Glob Planet Chang 142:1–13

Gu X, Zhang Q, Singh VP, Liu L, Shi P (2017a) Spatiotemporal patterns of annual and seasonal precipitation extreme distributions across China and potential impact of tropical cyclones. Int J Climatol 37(10):3949–3962

Gu X, Zhang Q, Singh VP, Shi P (2017b) Nonstationarity in timing of extreme precipitation across China and impact of tropical cyclones. Glob Planet Chang 149:153–165

Hu D, Saito Y, Kempe S (1998) Sediment and nutrient transport to the coastal zone. In: Galloway JN, Mellilo JM (eds) Asian change in the context of global climate change: impact of natural and anthropogenic changes in Asia on global biogeochemical cycles. IGBP Publ. Series, vol 3. Cambridge University Press, Cambridge, pp 245–270

IPCC (2007) Summary for policymakers of climate change 2007: the physical science basis, Contribution of Working Group I to the Fourth Assessment Report of the Intergovernmental Panel on Climate Change. Cambridge University Press, Cambridge

IPCC (2012) Summary for policymakers. In: Field CB, Barros V, Stocker TF, Qin D, Dokken DJ, Ebi KL, Mastrandrea MD, Mach KJ, Plattner G-K, Allen SK, Tignor M, Midgley PM (eds) Managing the risks of extreme events and disasters to advance climate change adaptation. A Special Report of Working Groups I and II of the Intergovernmental Panel on Climate Change. Cambridge University Press, Cambridge and New York, pp 3–21

Johnson RW (2001) An introduction to the bootstrap. Teach Stat 23(2): 49–54

Kao SC, Ganguly AR (2011) Intensity, duration, and frequency of precipitation extremes under 21st-century warming scenarios. J Geophys Res Atmos (1984-2012)

Kendon EJ, Roberts NM, Fowler HJ, Roberts MJ, Chan SC, Senior CA (2014) Heavier summer downpours with climate change revealed by weather forecast resolution model. Nat Clim Chang 4(7):570–576

Kharin VV, Zwiers FW (2005) Estimating extremes in transient climate change simulations. J Clim 18(8):1156–1173

Kharin VV, Zwiers FW, Zhang XB, Hegerl GC (2007) Changes in precipitation and temperature extremes in the IPCC ensemble of global coupled model simulations. J Clim 20(8):1419–1444

Knutson TR, McBride JL, Chan J, Emanuel K, Holland G, Landsea C, Held I, Kossin JP, Srivastava AK, Sugi M (2010) Tropical cyclones and climate change. Nat Geosci 3(3):157–163

Lai C, Shao Q, Chen X, Wang Z, Zhou X, Yang B, Zhang L (2016) Flood risk zoning using a rule mining based on ant colony algorithm. J Hydrol 542:268–280

Lai C, Zhong R, Wang Z, Wu X, Chen X, Wang P, Lian Y (2019) Monitoring hydrological drought using long-term satellite-based precipitation data. Sci Total Environ 649:1198–1208

Lima CHR, Kwon HH, Kim JY (2016) A Bayesian beta distribution model for estimating rainfall IDF curves in a changing climate. J Hydrol 540:744–756

Liu MX, Xu XL, Sun AY, Wang K, Liu W, Zhang X (2014) Is southwestern China experiencing more frequent precipitation extremes? Environ Res Lett 9(6):064002

Liu MX, Xu XL, Sun A (2015) Decreasing spatial variability in precipitation extremes in southwestern China and the local/large-scale influencing factors. J Geophys Res Atmos 120(13):6480–6488

Meehl GA, Karl T, Easterling DR, Changnon S, Pielke R, Changnon D, Evans J, Groisman PY, Knutson TR, Kunkel KE, Mearns LO, Parmesan C, Pulwarty R, Root T, Sylves RT, Whetton P, Zwiers F (2000) An introduction to trends in extreme weather and climate events: observations, socioeconomic impacts, terrestrial ecological impacts, and model projections. Bull Am Meteorol Soc 81(3):413–416

Milly PCD, Betancourt J, Falkenmark M, Hirsch RM, Kundzewicz ZW, Lettenmaier DP, Stouffer RJ (2008) Climate change-stationarity is dead: whither water management? Science 319(5863):573–574

Min SK, Zhang XB, Zwiers FW, Hegerl GC (2011) Human contribution to more-intense precipitation extremes. Nature 470(7334):378–381

NMIC (2012) Assessment report of China's ground precipitation 0.5° × 0.5° gridded dataset (V2.0). National Meteorological Information Center: Beijing

Pall P, Allen MR, Stone DA (2007) Testing the Clausius–Clapeyron constraint on changes in extreme precipitation under CO2 warming. Clim Dyn 28(4):351–363

Parmesan C (2006) Ecological and evolutionary responses to recent climate change. Annu Rev Ecol Evol Syst 37:637–669

Pinto I, Lennard C, Tadross M, Hewitson B, Dosio A, Nikulin G, Panitz HJ, Shongwe ME (2016) Evaluation and projections of extreme precipitation over southern Africa from two CORDEX models. Clim Chang 135(3–4):655–668

Rashid MM, Beecham S, Chowdhury RK (2016) Simulation of extreme rainfall and projection of future changes using the GLIMCLIM model. Theor Appl Climatol 130(1–2):453–466

Ren ZG, Zhang MJ, Wang SJ, Qiang F, Zhu XF, Dong L (2015) Changes in daily extreme precipitation events in South China from 1961 to 2011. J Geogr Sci 25(1):58–68

Sillmann J, Stjern CW, Myhre G, Forster PM (2017) Slow and fast response of mean and extreme precipitation to different forcing in CMIP5 simulations. Geophys Res Lett 44(12):6383–6390

Singh V, Goyal MK (2016) Spatio-temporal heterogeneity and changes in extreme precipitation over eastern Himalayan catchments India. Stochastic Environ Res Risk Assess 31(10):2527–2546

Singh J, Vittal H, Karmakar S, Ghosh S, Niyogi D (2016) Urbanization causes nonstationarity in Indian summer monsoon rainfall extremes. Geophys Res Lett 43(21):11269–11277

So BJ, Kim JY, Kwon HH, Lima CHR (2017) Stochastic extreme downscaling model for an assessment of changes in rainfall intensity-

duration-frequency curves over South Korea using multiple regional climate models. J Hydrol 553:321–337
Son C, Lee T, Kwon HH (2017) Integrating nonstationary behaviors of typhoon and non-typhoon extreme rainfall events in East Asia. Sci Rep 7:5097
Sraj M, Viglione A, Parajka J, Bloschl G (2016) The influence of non-stationarity in extreme hydrological events on flood frequency estimation. J Hydrol Hydromech 64(4):426–437
Stennett-Brown RK, Jones JJP, Stephenson TS, Taylor MA (2017) Future Caribbean temperature and rainfall extremes from statistical downscaling. Int J Climatol 37(14):4828–4845
Stocker T, Qin D, Plattner G, Tignor M, Allen S, Boschung J, Nauels A, Xia Y, Bex V, Midgley P (2013) IPCC, 2013: climate change 2013 the physical science basis: Contribution of Working Group I to the Fifth Assessment Report of the Intergovernmental Panel on Climate Change. https://doi.org/10.1017/CBO9781107415324
Sun J, Zhang FQ (2017) Daily extreme precipitation and trends over China. Sci Chin Earth Sci 60(12):2190–2203
Sun QH, Miao CY, Qiao YY, Duan QY (2017a) The nonstationary impact of local temperature changes and ENSO on extreme precipitation at the global scale. Clim Dyn 49(11–12):4281–4292
Sun QH, Miao CY, Duan QY (2017b) Changes in the spatial heterogeneity and annual distribution of observed precipitation across China. J Clim 30(23):9399–9416
Svensson C, Jones DA (2010) Review of methods for deriving areal reduction factors. J Flood Risk Manag 3(3):232–245
Um MJ, Kim Y, Markus M, Wuebbles DJ (2017) Modeling nonstationary extreme value distributions with nonlinear functions: an application using multiple precipitation projections for US cities. J Hydrol 552: 396–406
Ummenhofer CC, Meehl GA (2017) Extreme weather and climate events with ecological relevance: a review. Philos Trans R Soc Lond 372(1723):20160135
Wang WG, Shao QX, Yang T, Peng SZ, Yu ZB, Taylor J, Xing WQ, Zhao CP, Sun FC (2013) Changes in daily temperature and precipitation extremes in the Yellow River Basin, China. Stochastic Environ Res Risk Assess 27(2):401–421
Wang Z, Lai C, Chen X, Yang B, Zhao S, Bai X (2015) Flood hazard risk assessment model based on random forest. J Hydrol 527:1130–1141
Wang R, Chen JY, Chen XW, Wang YF (2017a) Variability of precipitation extremes and dryness/wetness over the southeast coastal region of China, 1960-2014. Int J Climatol 37(13):4656–4669
Wang Z, Xie P, Lai C, Chen X, Zeng Z, Li J (2017b) Spatiotemporal variability of reference evapotranspiration and contributing climatic factors in China during 1961-2013. J Hydrol 544:97–108
Wang Z, Zeng Z, Lai C, Lin W, Wu X, Chen X (2017c) A regional frequency analysis of precipitation extremes in Mainland China with fuzzy c-means and L-moments approaches. Int J Climatol 37:429–444
Wang Z, Zhong R, Lai C, Zeng Z, Lian Y, Bai X (2018a) Climate change enhances the severity and variability of drought in the Pearl River Basin in South China in the 21st century. Agric For Meteorol 249: 149–162
Wang Z, Li J, Lai C, Wang RY, Chen X, Lian Y (2018b) Drying tendency dominating the global grain production area. Glob Food Sec 16: 138–149
Westra S, Alexander LV, Zwiers FW (2013) Global increasing trends in annual maximum daily precipitation. J Clim 26(11):3904–3918
Wong KK, Zhao XB (2001) Living with floods: victims' perceptions in Beijiang, Guangdong, China. Area 33(2):190–201
Wu CH, Huang GR (2015) Changes in heavy precipitation and floods in the upstream of the Beijiang River Basin, South China. Int J Climatol 35(10):2978–2992
Wu XS, Wang ZL, Zhou XW, Lai CG, Lin WX, Chen XH (2016) Observed changes in precipitation extremes across 11 basins in China during 1961-2013. Int J Climatol 36(8):2866–2885
Yin H, Donat MG, Alexander LV, Sun Y (2015) Multi-dataset comparison of gridded observed temperature and precipitation extremes over China. Int J Climatol 35(10):2809–2827
You QL, Kang SC, Aguilar E, Pepin N, Flugel WA, Yan YP, Xu YW, Zhang YJ, Huang J (2011) Changes in daily climate extremes in China and their connection to the large scale atmospheric circulation during 1961-2003. Clim Dyn 36(11–12):2399–2417
Zhang XB, Zwiers FW, Hegerl GC, Lambert FH, Gillett NP, Solomon S, Stott PA, Nozawa T (2007) Detection of human influence on twentieth-century precipitation trends. Nature 448(7152):461–465
Zhang Q, Singh VP, Li JF, Chen XH (2011a) Analysis of the periods of maximum consecutive wet days in China. J Geophys Res Atmos 116:D23106
Zhang XB, Alexander L, Hegerl GC, Jones P, Tank AK, Peterson TC, Trewin B, Zwiers FW (2011b) Indices for monitoring changes in extremes based on daily temperature and precipitation data. Wiley Interdiscip Rev Clim Chang 2(6):851–870
Zhang DL, Lin YH, Zhao P, Yu XD, Wang SQ, Kang HW, Ding YH (2013) The Beijing extreme rainfall of 21 July 2012: "right results" but for wrong reasons. Geophys Res Lett 40(7):1426–1431
Zhang ZJ, Zhang CM, Cui QR (2017) Random threshold driven tail dependence measures with application to precipitation data analysis. Stat Sin 27(2):685–709
Zhou BT, Wen QH, Xu Y, Song LC, Zhang XB (2014) Projected changes in temperature and precipitation extremes in China by the CMIP5 multimodel ensembles. J Clim 27(17):6591–6611
Zhu Q, Xu YP, Gu H (2016) Parameter uncertainty and nonstationarity in regional extreme rainfall frequency analysis in Qu River Basin, East China. J Hydrol Eng 21(5):04016008
Zong YQ, Chen XQ (2000) The 1998 flood on the Yangtze, China. Nat Hazards 22(2):165–184